

UNCLASSIFIED

AD 408 205

DEFENSE DOCUMENTATION CENTER

FOR

SCIENTIFIC AND TECHNICAL INFORMATION

CAMERON STATION, ALEXANDRIA, VIRGINIA



UNCLASSIFIED

634-2

408 205

ASD-TDR-63-118

CATALOGED BY DDC
AS AD No. 408205

RATE-LIMITING STEPS ON FUEL-CELL ELECTRODES
TECHNICAL DOCUMENTARY REPORT ASD-TDR-63-118

JANUARY 1963

FLIGHT ACCESSORIES LABORATORY
AERONAUTICAL SYSTEMS DIVISION
AIR FORCE SYSTEMS COMMAND
WRIGHT-PATTERSON AIR FORCE BASE, OHIO

Project No. 8173, Task No. 817306

(Prepared under Contract No. AF 33(616)-7624
by Massachusetts Institute of Technology,
Research Laboratory of Electronics,
Energy Conversion Group,
Cambridge, Massachusetts.
Author: Adrian R. Reti)

DDC
JUN 24 1963
IAISIA R

ABSTRACT

The purpose of this investigation was to identify and to study the step or steps that limit fuel cell electrode performance. The electrodes considered were the typical porous, gaseous diffusion type, and most of the effort was directed toward acquiring a more quantitative understanding of the effect of the different variables governing electrode performance.

Since it is necessary to be able to predict quantitatively both the mass transfer and the kinetic limitations in order to calculate electrode performances, an experimental program directed toward obtaining the necessary kinetic data for systems of interest was undertaken. An experimental system was devised by means of which the electrochemical kinetics could be studied over a wide current density range independently of mass transfer effects, on electrodes of known catalyst area. In the operating region where the effect of mass transfer became significant, it was possible quantitatively to assess its importance.

It was found that for all of the systems studied (O_2 and H_2O_2 electroreduction, H_2 and ethylene oxidation), for a particular catalyst-electrolyte system, the electrode performance could be described as a function of reactant concentration and current density only. The most significant finding in these electrochemical kinetic studies was that for both the O_2 and the H_2 systems, in the current density range of practical interest (10^{-2} to 10^{-4} amp/cm²) the reactant chemisorption rate on the electrode surface plays an important role in governing the electrode potential, and makes it impossible to describe the electrode performance by a simple expression such as the Tafel equation.

Electrode performance calculations were made for the case of an oxygen electrode of idealized geometry, by using the experimentally obtained kinetic data and the known values of oxygen solubilities and diffusivities in liquid electrolytes. It was found that if the electrode geometrical parameters (pore size distribution, location, etc.) are properly chosen, electrode performances much superior to the ones thus far obtained by several investigators should be possible, showing that the potential performance of such types of electrodes has not yet been fully realized.

PUBLICATION REVIEW

The publication of this report does not constitute approval by the Air Force of the findings or conclusions contained herein. It is published for the exchange and stimulation of ideas.

GLOSSARY

<u>Symbol</u>	<u>Definition</u>
A	Constant in adsorption equation
a	Constant in Tafel equation
B	Constant in adsorption equation
b	Constant in Tafel equation
C_D	Capacitance of dummy electrode D_{Ac} (Fd)
C_{DL}	Specific electrical double-layer capacitance (Fd/cm ²)
C_S	Capacitance of electrode system (Fd)
C_T	Capacitance of test electrode T (Fd)
c_o	Reactant concentration at gas-liquid interface (g. moles/cm ³)
c_s	Reactant concentration at electrode surface (g. moles/cm ³)
c_x	Reactant concentration at a distance x within a pore (g. moles/cm ³)
C_p	Specific heat (Btu/lb °F)
D	Macropore diameter (cm)
d	Micropore diameter (cm)
D_L	Liquid-phase diffusivity (cm ² /sec)
E_{act}	Measured electrode potential (volts)
E_{rev}	Reversible theoretical electrode potential (volts)
E_o	Standard electrode potential (volts)
F	Faraday's constant, 96,500 coulombs/gram equivalent
h	Heat-transfer coefficient (Btu/hr ft ² °F)
I	Current (amps)
i_F	Face-area current density (amp/cm ² electrode face area)
i_L	Limiting current density (amp/cm ²)
i_{Tot}	Total current density (amp/cm ² of total electrode area)
i_S	Surface current density (amp/cm ² of electrode active surface)
k	Thermal conductivity (Btu/hr ft °F)
k_L	Liquid-phase mass-transfer coefficient (cm/sec)

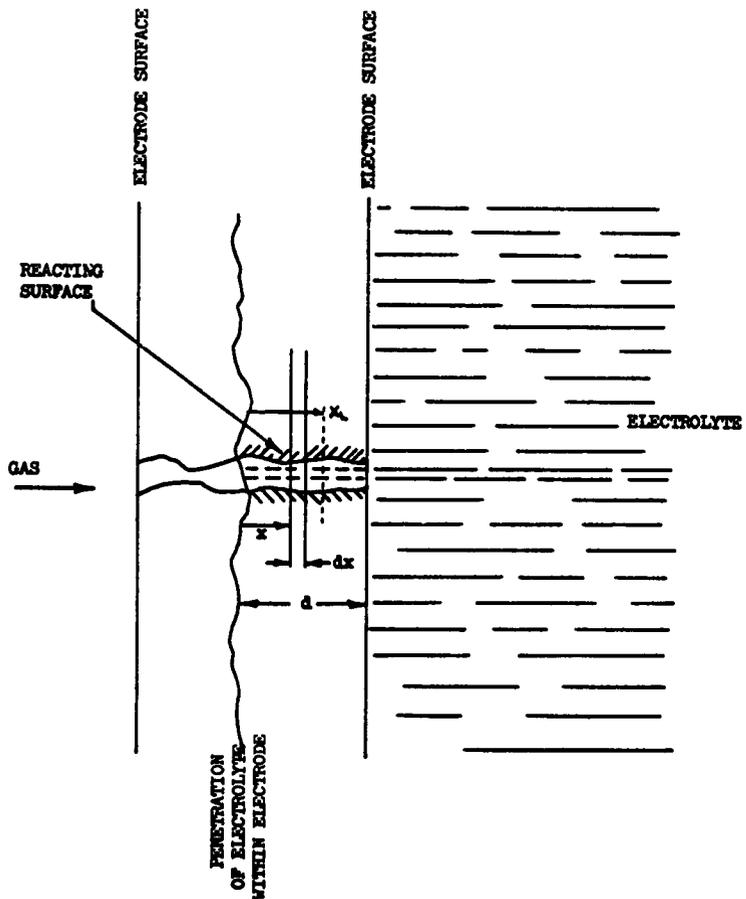


Fig. 1. Illustration of porous system.

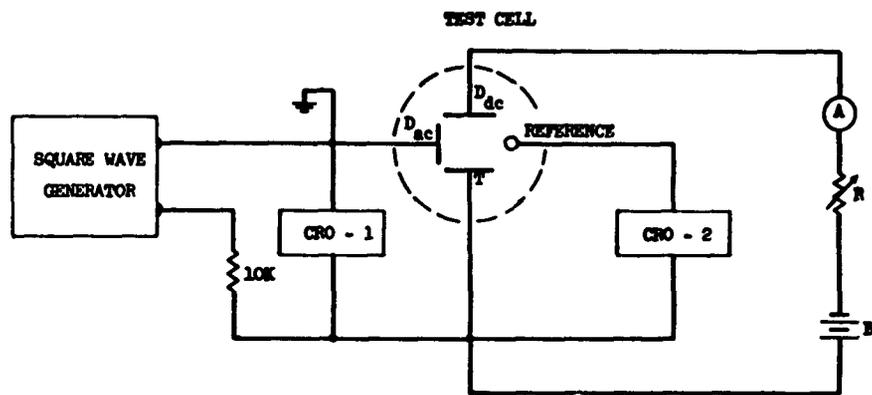


Fig. 3. Circuit for the double-layer capacitance measurements.

3.2 ELECTROCHEMICAL KINETICS

a. Oxygen Electroreduction

Several experiments have been performed to study the oxygen electroreduction reaction on both silver and platinum wire screens, under conditions of varying flow, pH, temperature, and current density. The results are presented in electrode potential (versus the Standard Hydrogen Electrode, S.H.E.) vs current density graphs, the current density being plotted on a logarithmic scale, in order to show the electrode behavior over an adequately wide current-density range.

Typical Effects of O₂ Concentration and Electrolyte Flow Rate

Figures 5 and 6 show the effects of electrolyte-oxygen concentration and electrolyte flow velocity for platinum- and silver-screen electrodes, respectively. These runs were performed under such conditions that even at the highest current density no more than 10% of the oxygen in the flowing electrolyte was consumed, in order to have a constant oxygen-diffusion driving force throughout the electrode.

The results are quite similar for the two different metal electrodes. All of the voltage-log current-density curves shown here are characterized by an initial straight-line region at very low currents, followed by a region in which the overvoltages become greater at a progressively increasing rate, up to a point where the voltage-log current-density curve becomes nearly vertical. For each electrode we also find that the straight-line portion of these curves at low current densities is common to all runs, independently of oxygen concentration or electrolyte flow velocity; that is to say, the electrode potential is a function of current density only, and not of the oxygen supply conditions. The vertical portion of the curves, on the other hand, is strongly dependent on the oxygen concentration in the electrolyte and on the electrolyte flow velocity. Runs with electrolyte saturated at 1.0 atm with pure oxygen and with air ($p_{O_2} = 0.21$ atm) in which the electrolyte flows at the same space velocity through the screens for both cases, show that the location of this vertical region or drop-off in the curves differs by a factor of approximately 5 in the current-density scale, which would be expected if the oxygen mass-transfer rate from bulk electrolyte to the electrode surface were controlling. Runs at different electrolyte flow rates also show that the current density at this vertical region increases with a power dependence that is between the 0.6^{th} and the first power of the liquid flow rate.

Calculation of the oxygen mass-transfer rates to the electrode surface from values of oxygen solubility and diffusivity in potassium hydroxide that have been reported, and measured flow rates are listed in Appendix A. The results are presented in Table 1. These calculated limiting current densities check with the observed limiting current-density values, especially if we consider that the diffusivity and the solubility of O₂ in 20% KOH are not known very accurately, and if we take into account the approximations made in the mass-transfer calculations (approximating a screen system that flows

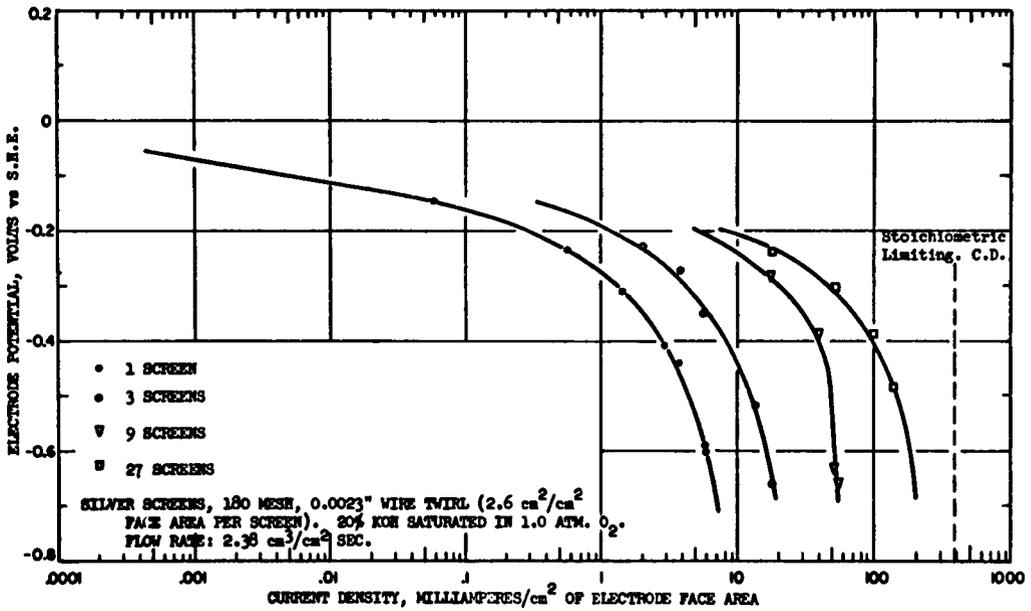


Fig. 9. Experiments with multiple screens.

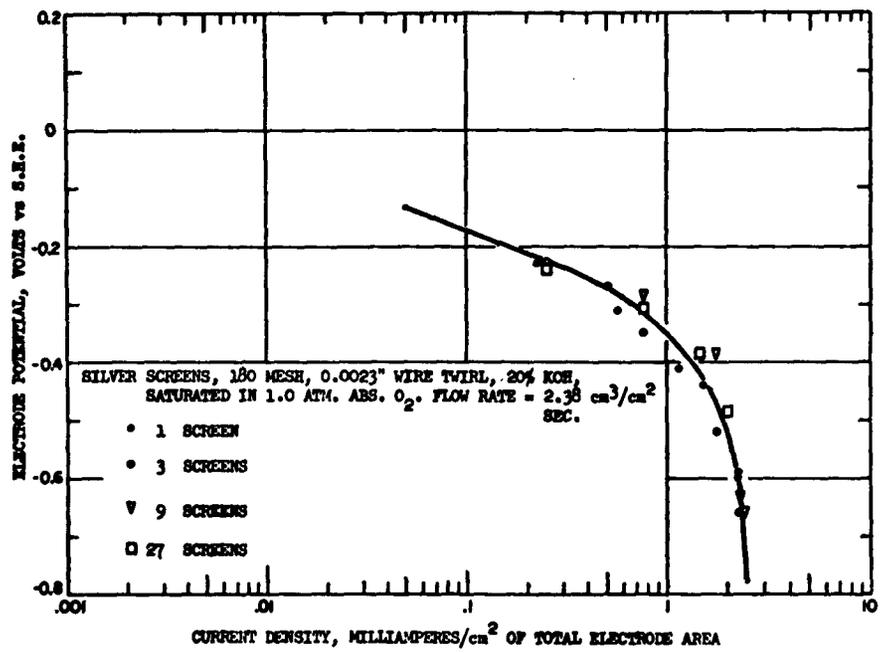


Fig. 10. Experiments with multiple screens.

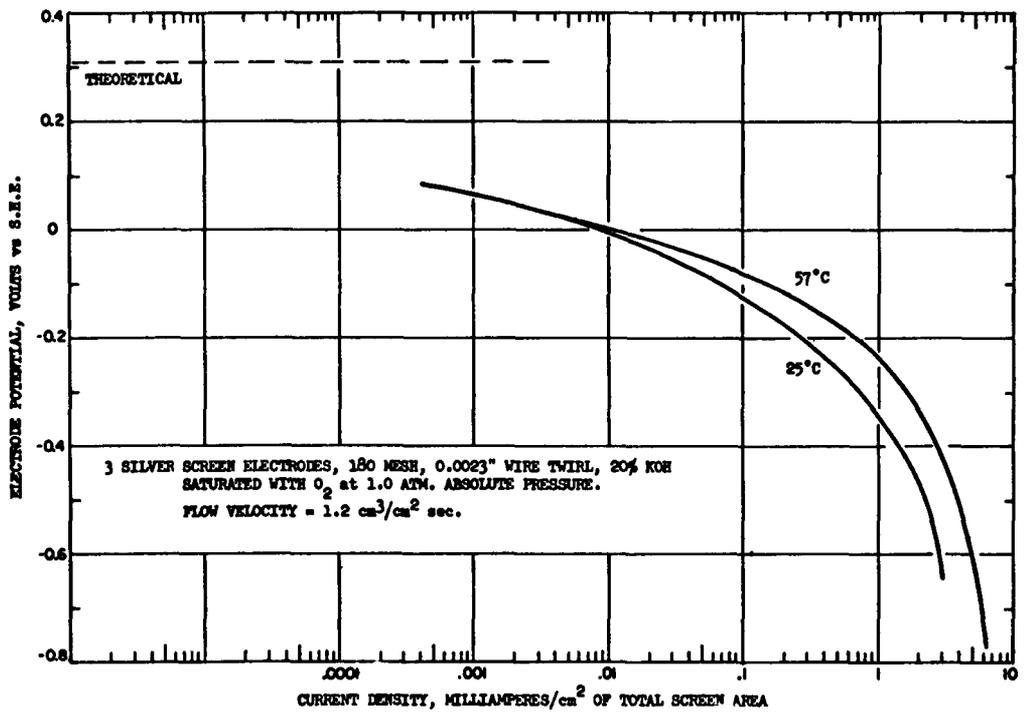


Fig. 11. Effect of temperature on electrode performance.

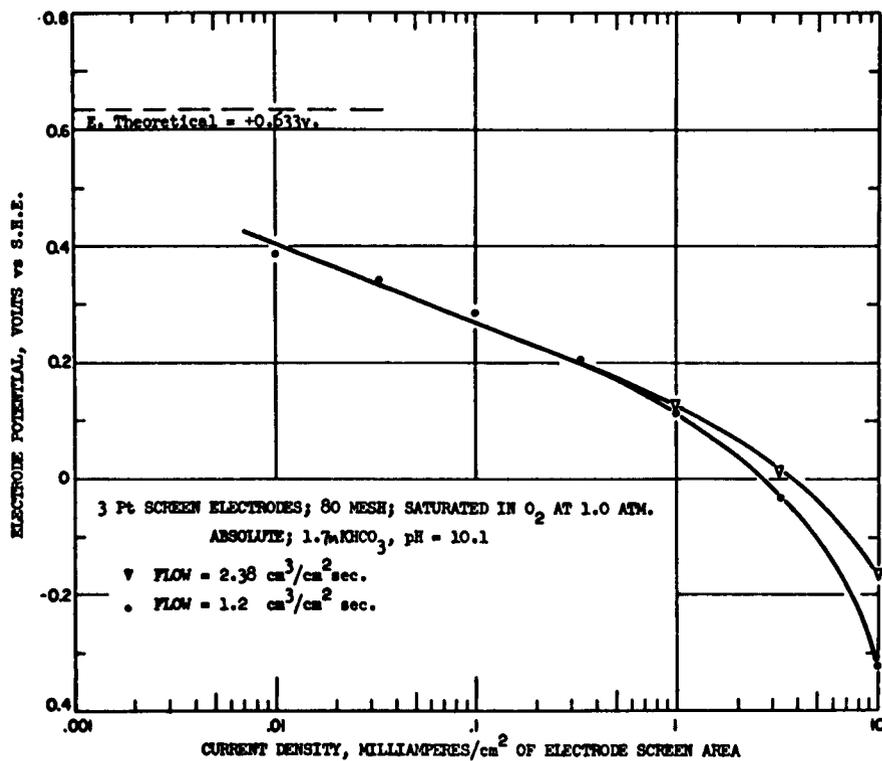


Fig. 12. Oxygen electroreduction on platinum at pH = 10.1.

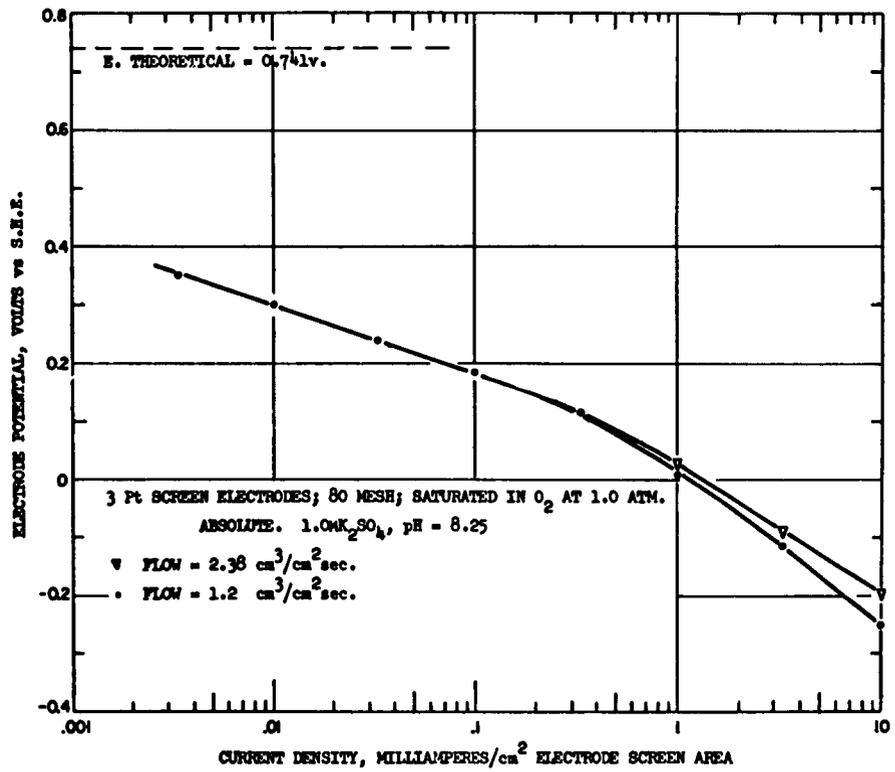


Fig. 13. Oxygen electroreduction on platinum at pH = 8.25.

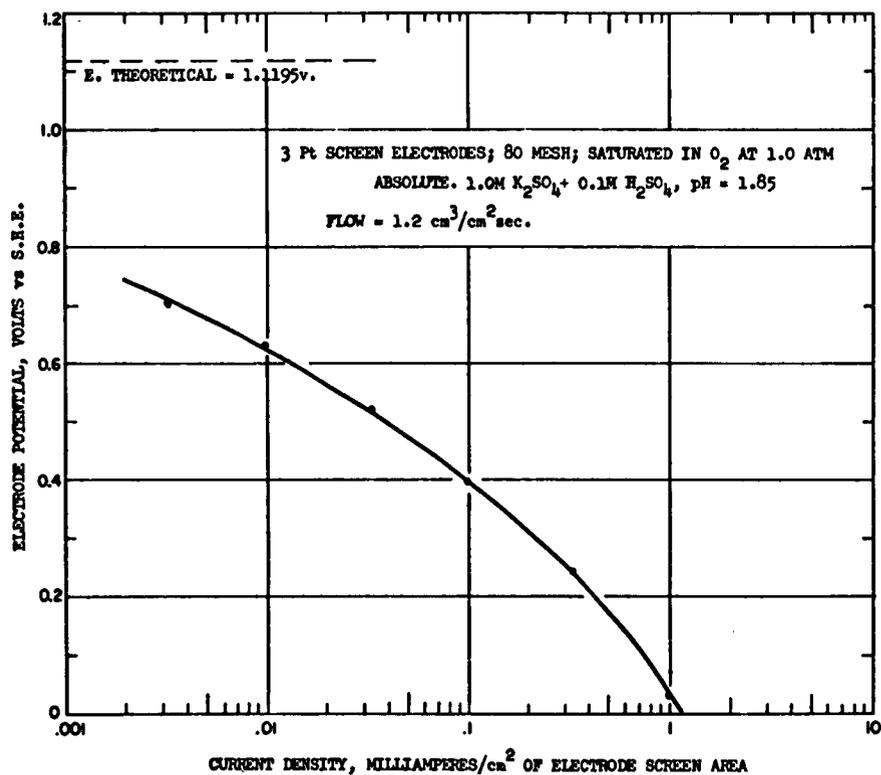


Fig. 14. Oxygen electroreduction on platinum at pH = 1.85.

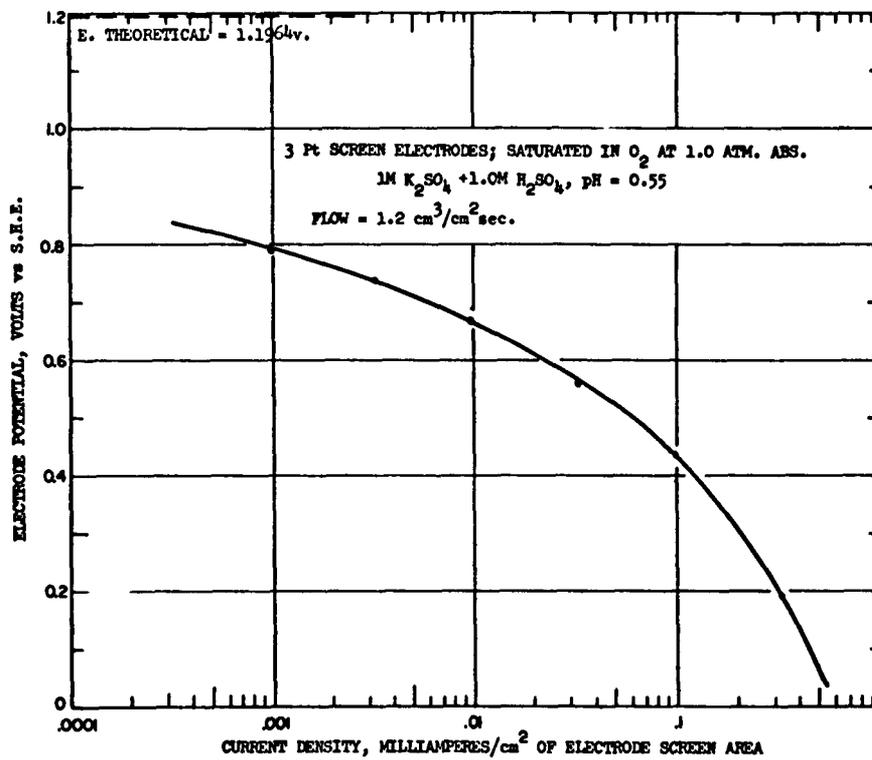


Fig. 15. Oxygen electroreduction on platinum at pH = 0.55.

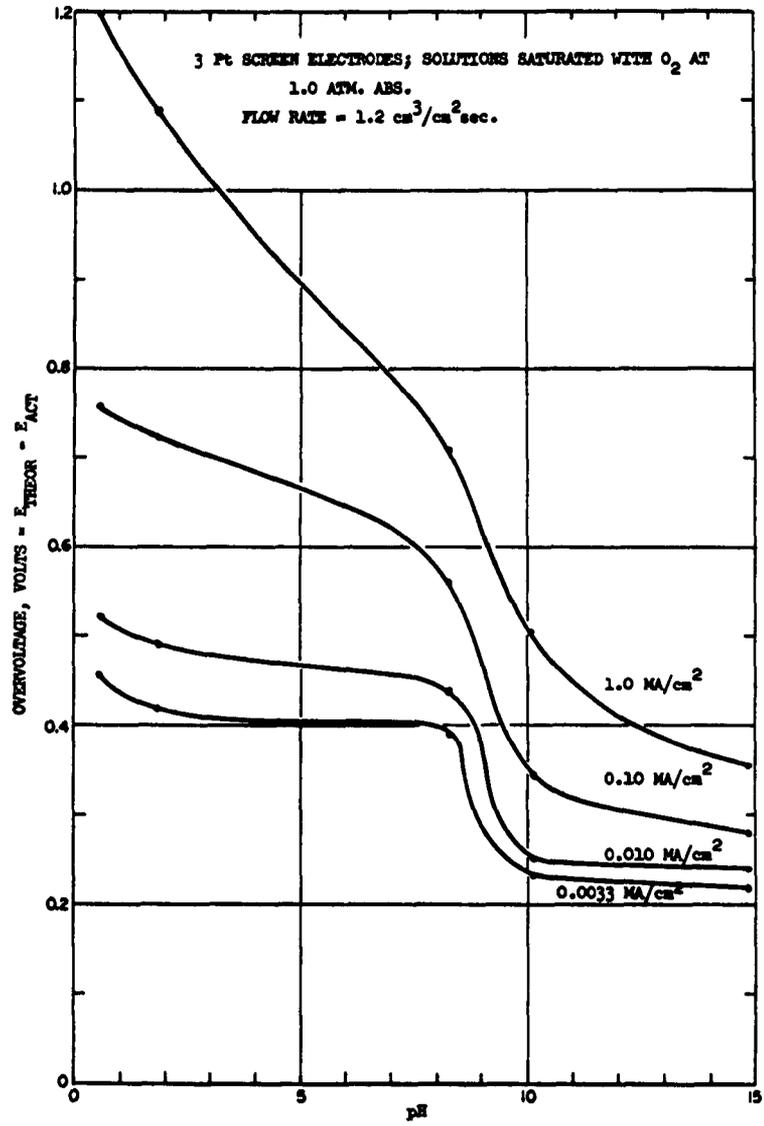


Fig. 16. Oxygen electroreduction overvoltage on platinum electrodes.

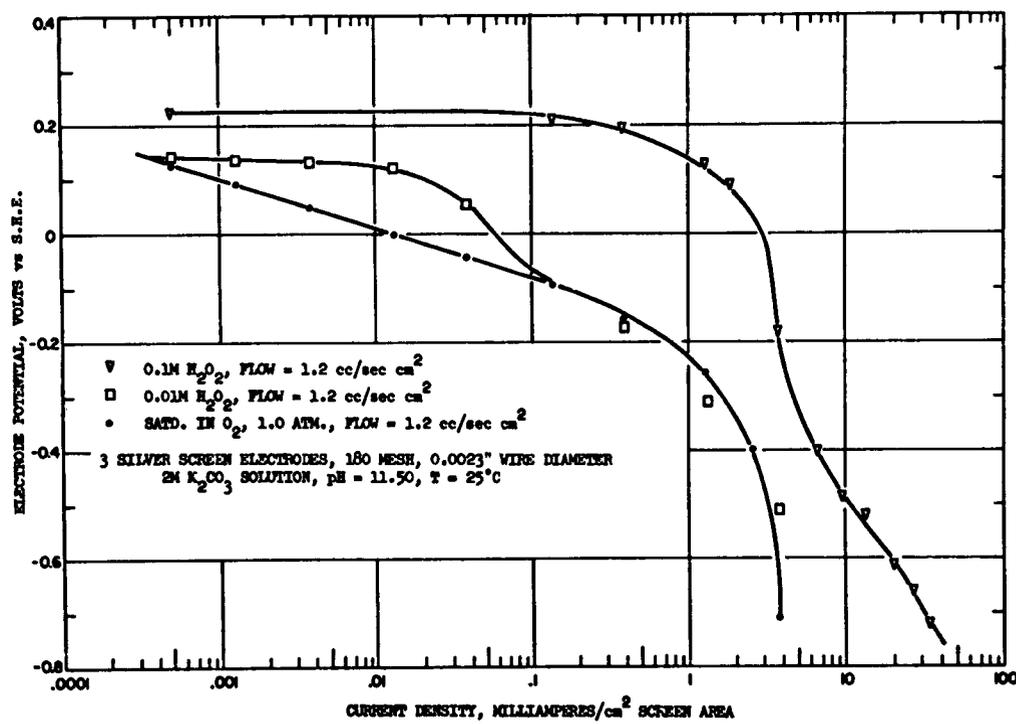


Fig. 20. Hydrogen peroxide electroreduction on silver at pH = 11.50.

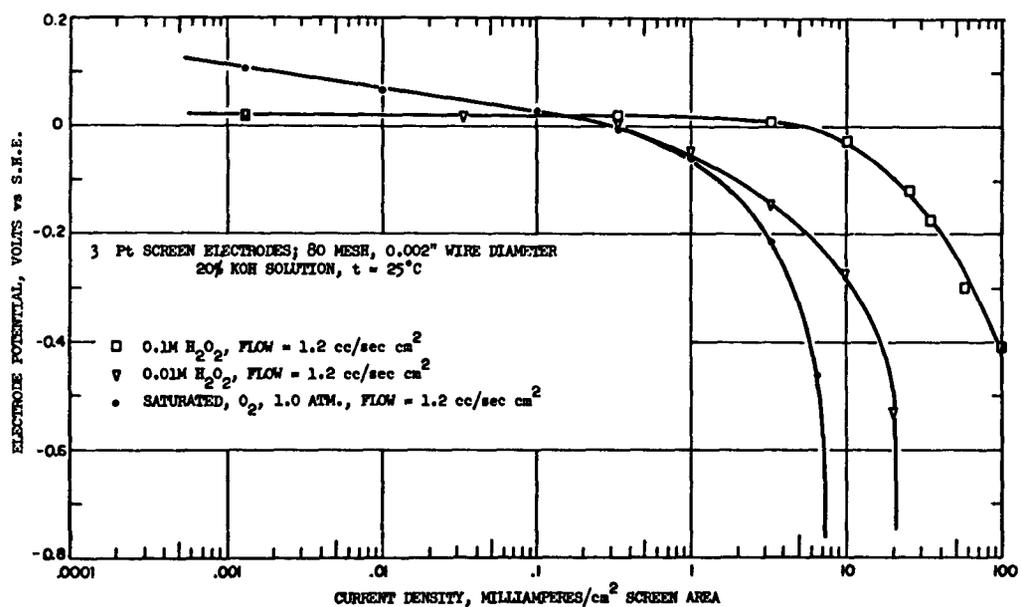


Fig. 22. Hydrogen peroxide electroreduction on platinum in 20% KOH.

It can be observed from these results that in both cases the electrode potential is constant and equal to the open-circuit potential up to fairly high current densities (0.05 ma/cm^2 in base, and 0.01 ma/cm^2 in acid). This fact is consistent with the observations of other authors that the hydrogen-electrode reaction does have a high exchange-current density, of the order of 10^{-4} amp/cm^2 . The reversibility of the hydrogen electrode in this low-current-density region is evident from comparison of the observed electrode potentials with the calculated reversible potentials for both solutions: in basic solution the observed potential is within 12 mv of the theoretical potential, and in acid solution the difference is only 24 mv. Such a difference is within the limits of the experimental error, if we consider that the calomel reference electrode potential is known only within 20 mv, because of liquid-junction potential effects that are not taken into account in this work.

As the current density is increased, a region is reached where the hydrogen-electrode potential is dependent on the hydrogen-supply conditions (hydrogen concentration and saturated electrolyte flow rate), just as in the oxygen-electrode studies. The limiting current densities are of the order of magnitude expected from mass-transfer calculations; therefore we see that hydrogen concentration polarization is responsible for the final sharp rise in potential. Again, as in the case of the oxygen electrode, the transition from pure electrochemical kinetics governing the electrode potential to concentration polarization is not as sharp as would be expected from theory, if these were the only two phenomena taking place. These results suggest that the rate of hydrogen chemisorption on the platinum surface is influencing the electrode behavior, if we use the same arguments presented in the case of the oxygen electrode.

It is clear that the electrochemical kinetics per se is not limiting the electrode performance. Furthermore, the electrochemical kinetics for this reaction has been studied in great detail by many authors, and emphasis on this type of study is not necessary. From the results obtained, however, it appears that in order to calculate the hydrogen-electrode performance more must be known about the rate of hydrogen adsorption on the electrode surface, and its influence on electrode performance. Such a study was not possible for the present work because it was not possible to vary the hydrogen partial pressure through a wide enough range, mainly at pressures above 1 atmosphere, to yield useful results.

d. Ethylene Oxidation Studies

Experiments directed toward the investigation of the electrochemical oxidation of ethylene on platinum screens in $1M \text{ KHCO}_3$ and $0.5M \text{ H}_2\text{SO}_4$ solutions were performed. We found that this reaction takes place with such difficulty in both cases that no reliable data could be obtained. High polarizations were encountered at current densities of approximately $0.1 \mu\text{amp}$ per square centimeter, and thus any study of this electrode process should be conducted in an experimental system in which the presence of even traces ($10^{-10} \text{ g moles/cc}$) of oxygen is eliminated. The experimental system used was

and hydrated ions that are being transported. Furthermore, there is a minimum spacing between pores set by structural considerations which fixes the maximum number of pores present.

Recognizing these limitations, it is possible for us to calculate the theoretically attainable performance of various electrode structures. Assume that the electrode is a flat plate containing a multiplicity of cylindrical pores, somewhat along the lines of Austin¹ as shown in Fig. 1. These pores are at right angles to the electrode face, are evenly distributed with a distance of two diameters from center to center, and assumed to be filled with liquid so that the gas-liquid interface lies somewhere within the pore. The adoption of such an idealized geometry simplifies the calculations, but still gives results that are quite applicable to less uniform geometries.

In order to calculate the total amount of oxygen that is being reduced throughout the pore at a given overvoltage, the pore wall can be treated as an equipotential surface; this is a good assumption as the electrode material (platinum or silver in this case) is a good conductor. The current density at any point within the pore will be determined by the oxygen concentration at that point, and this concentration can be obtained by a finite differences calculation throughout the pore, starting at a point where essentially a very low oxygen concentration exists, and calculating step by step the concentration increases (and consequent current-density increases) as the pore mouth is approached. A typical calculation of this kind is presented in Appendix D.

The results of such an analysis for a porous system of 30 Å pore diameter, platinum catalyst surface, oxygen at 1 atm partial pressure at the pore mouths, and 60 Å pore spacing are shown in Fig. 29. This performance is not yet very attractive, hence the electrode model just presented must be revised to increase even further the amount of electrode surface available for electrochemical reaction. By use of macropores from each of which the small micropores radiate, the number of micropores per unit of electrode face area increases greatly. Such a geometry is sketched in Fig. 30. In considering the spacing, diameter, and depth of these macropores, the following factors are relevant:

(a) The interpore wall thickness should be approximately twice the "active length" of the micropores, so that all micropores can function properly.

(b) Liquid penetration into the porous structure should be small enough to avoid large IR drops within the electrolyte in the pores.

The first consideration determines the diameter of the macropores to be approximately 4 microns, since from the calculation outlined above it is found that appreciable reaction occurs within the micropores for a length of approximately 2 microns. For the case under consideration, the resistivity of 20% KOH at 25°C is 2 ohm-cm. In the given geometry, the porosity of the solid microporous structure will be

$$\epsilon = \frac{\pi d^2}{4(2d)^2} = 0.196.$$

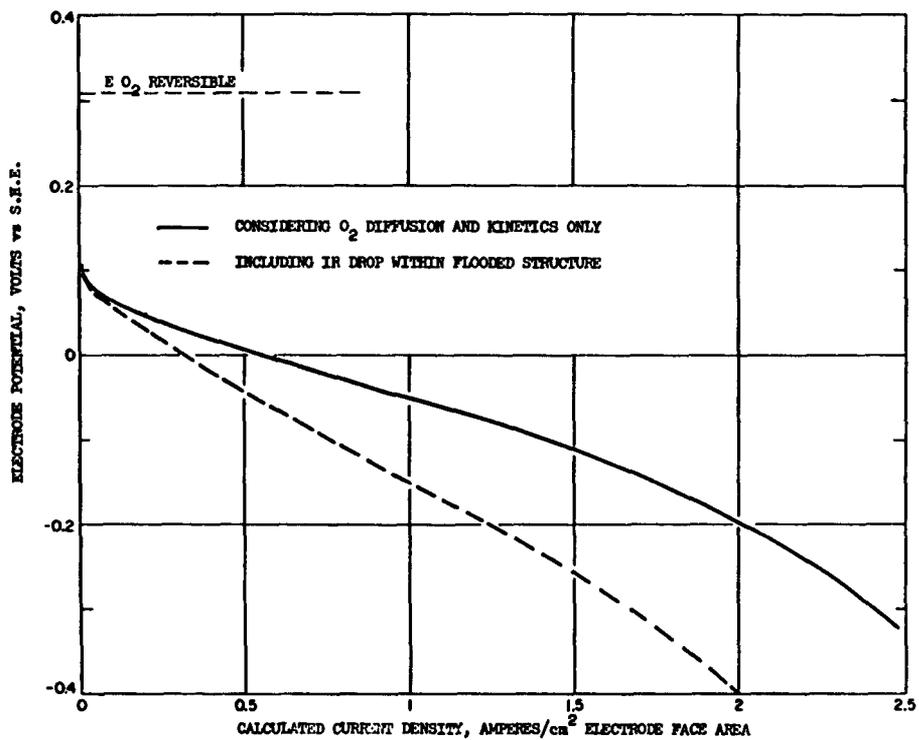


Fig. 31. Calculated performance for the microporous-macroporous structure of Fig. 30.

Since the micropores in an actual case are not straight, a tortuosity path q of approximately 2 (a typical number for porous systems) may be considered. The effective resistivity¹ of the flooded microporous material is

$$\rho_{\text{eff}}^1 = \rho_{\text{free}}^1 \frac{q}{\epsilon} = \frac{(2)(2)}{0.196} = 20.4 \text{ ohms-cm.}$$

The resistivity of the layer as a whole, if we take into account the existence of nonconducting, nonflooded macropores (the tortuosity path factor here will be negligible, since the "flooded solid" occupies approximately 80% of the total volume) is

$$\rho' = \frac{20.4}{(1-0.196)} = 25.4 \text{ ohms-cm}$$

if the macropores are spaced two diameters from center to center as well.

If we consider a reasonable IR drop within the electrode to be 0.1 volt at 1.0 amp/cm² of electrode face area, the thickness of this active layer will be

$$L_{\text{R}} = \frac{2(\Delta V)}{I_{\text{F}} R} = \frac{2(0.1)}{1.0(25.4)} = 0.00786 \text{ cm,}$$

under the assumption that the current is nearly uniformly generated throughout the macropore.

The face area of the flooded microporous material per unit electrode face area will then be

$$\frac{\text{number of macropores}}{\text{cm}^2 \text{ electrode face area}} (\text{effective area of macropore})$$

$$= \frac{\pi DL}{4(2D)^2} = \frac{\pi(0.00786)}{4(4) 10^{-4}} = 15.5 \text{ cm}^2/\text{cm}^2.$$

The calculated electrode current density per unit electrode face area for the micro-macropore structure is shown in Fig. 31. The lower performance curve of Fig. 31 incorporates the effect of the IR drop through the flooded micropore area.

This calculated performance curve has the same general shape as the experimental curve obtained for porous gas-diffusion electrodes by many investigators.^{7,37} One interesting point is that the calculated performance for this system, which has not been optimized, is higher than any electrode performances yet observed. This means that by building an electrode of the appropriate geometry, higher electrode performances than the ones at present observed should be attained. The calculations above also show the relative influence of the different operating and geometrical variables on electrode performance, and should be helpful in determining the optimal configuration for any given electrode system and operating conditions.

IV. CONCLUSIONS

The conclusions resulting from this investigation can be divided into two groups, one concerning findings on the electrode-kinetics studies, and the other referring to findings connected with the electrode-performance studies.

4.1 ELECTRODE KINETICS

For all electrodes studied, we found that for a given solution-electrode system, the electrode potential is uniquely determined by the reactant and reaction product concentration at the electrode surface, and the electrode current density.

The experimental method employed in these studies (flowing a reactant-saturated electrolyte past an electrode of known geometry) is particularly suited to the study of these specific reaction rates as a function of current density and reactant concentration, since from it reproducible and readily interpretable results can be obtained on the basis of current density per unit of actual electrode area.

a. Oxygen Electroreduction Reaction on Platinum and Silver

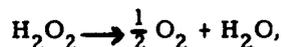
At very low current densities (10^{-7} - 10^{-4} amp/cm²) the electroreduction kinetics is the sole process that controls the electrode potential. In the current-density range of practical interest (10^{-4} - 10^{-2} amp/cm²), however, the oxygen chemisorption step is rate-limiting, and this results in abnormally high overvoltages (premature deviation from the Tafel line).

The oxygen electroreduction rate on platinum and silver electrodes decreases at a given overpotential as the solution pH is decreased. This change is most pronounced at a pH value of approximately 9.

b. Hydrogen Peroxide Electroreduction

The hydrogen peroxide electroreduction reaction has a high exchange-current density (from 10^{-2} amp/cm² to 2×10^{-4} amp/cm², which depends on the conditions), and very high specific current densities (up to 10^{-1} amp/cm² in 0.1M H₂O₂-20% KOH) can be obtained, with the electroreduction kinetics being the sole rate-controlling step at all times. There is no evidence that a chemisorption step is rate-controlling even at the highest current densities.

Since the hydrogen peroxide decomposes spontaneously at the electrode surface through the reaction



the oxygen electroreduction reaction takes place concurrently with the hydrogen peroxide electroreduction, and, in some cases, becomes the potential determining reaction.

c. Hydrogen Electro-oxidation

As other investigators have observed, the hydrogen electrode reaction is essentially reversible at low current densities, the open-circuit potential being equal to the theoretical reversible electrode potential. The exchange-current density for the hydrogen electrode reaction on platinum is high, of the order of 10^{-4} amp/cm², and thus electrochemical kinetics is not expected to be limiting under most circumstances.

In the current-density range of practical interest (10^{-2} - 10^{-4} amp/cm²) the hydrogen chemisorption step is rate-limiting, resulting in abnormally high overpotentials.

d. Ethylene Oxidation

The electrochemical oxidation rate of ethylene on platinum electrodes in 1M KHCO₃ and 0.5M H₂SO₄ solutions was found to be impractically low, resulting in high electrode polarization at current densities as low as 10^{-7} amp/cm². The electrode kinetics in this case is controlling the electrode potential at all times.

4.2 ELECTRODE-PERFORMANCE STUDIES

(i) The performance of a gaseous-diffusion electrode of idealized geometry can be calculated if the electrode kinetics is known as a function of electrode potential and reactant concentration.

(ii) In order to achieve satisfactory electrode performance, an electrode containing both electrolyte-flooded micropores (30-100 Å in diameter) and nonflooded macropores (1-10 microns in diameter) is necessary, in order to maximize the amount of electrode active area per unit of electrode face area.

(iii) In order to keep the ohmic drops within the electrode down to a reasonable value, the thickness of this "active" flooded micropore region must be of the order of 10^{-2} cm.

(iv) If such an idealized geometry is achieved, it should be possible to greatly increase the performance of gaseous-diffusion oxygen electrodes above the best performance that has been achieved thus far with the available catalyst materials.

V. RECOMMENDATIONS FOR FURTHER RESEARCH

On the basis of the findings made during this investigation, the following recommendations can be made in connection with further fuel-cell electrode research.

(i) Any electrode-kinetic studies directed toward oxygen or hydrogen electrode design or performance calculations should take into consideration the strong role played by the reactant chemisorption step in controlling the electrode-performance curve. The effect of a wide range of reactant concentrations at the electrode surface should be studied, to determine more quantitatively the limitations imposed by the chemisorption rate of the reacting species.

(ii) The development of a gaseous-diffusion electrode of a geometry similar to the one described in Fig. 30 should be undertaken, and the performance of such an electrode should be checked against the predicted performance.

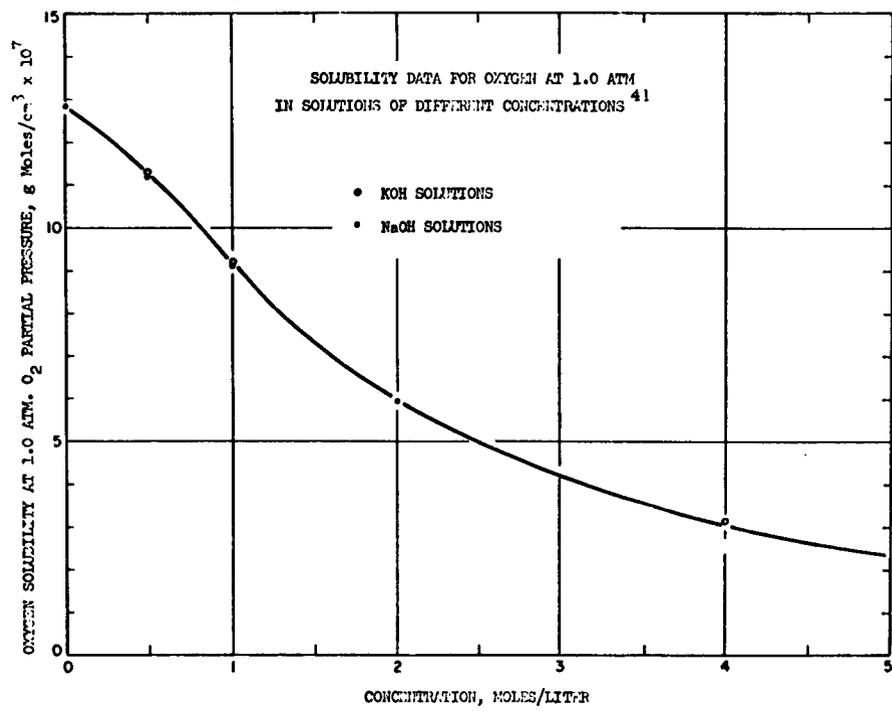


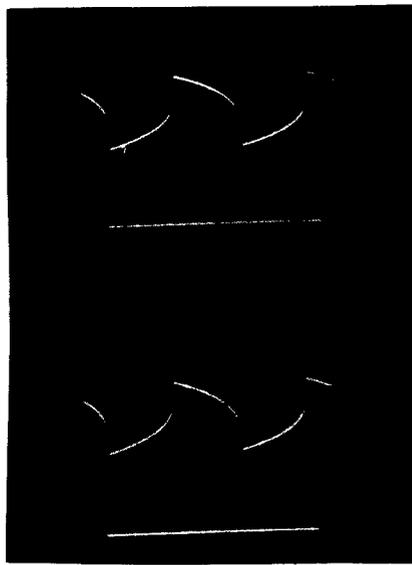
Fig. 32. Solubility data for oxygen at 1.0 atm in electrolyte.

$$I_L = \overset{4}{N_{O_2}} nF = 3.14 \times 10^{-2} (2.9 \times 10^{-7}) 4 (96,500) = 3.5 \times 10^{-3} \text{ A/cm}^2.$$

Case 4.

Same conditions as for Case 3, except that the solution is saturated in air at 1 atm ($p_{O_2} = 0.21 \text{ atm}$)

$$I_L = 3.5 \times 10^{-3} (0.21) = 0.736 \times 10^{-3} \text{ amp/cm}^2.$$



Charging-Curve Beam

Vertical axis, scale 500 microvolts/cm

Horizontal axis, scale 2×10^{-4} sec/cm

Electrode-Potential Monitoring Beam

Vertical axis, scale 0.100 volt/cm

Horizontal axis, scale 100 sweeps/sec

Calibration 0.00 volt at bottom of scale

Fig. 33. Double-layer charging curves.

The measured capacitance then is

$$C_T = I \frac{dt}{dv} = 5 \times 10^{-4} \frac{1}{0.915} = 5.48 \times 10^{-4} \text{ farad.}$$

Since the test-electrode surface area is 3.0 cm^2 , the electrical double-layer capacitance is

$$C_{DL} = \frac{5.48 \times 10^{-4} \times 10^6}{3.0} = 183 \mu\text{fd/cm}^2.$$

APPENDIX C

POROUS CARBON ELECTRODE PREPARATION

The Kordesh^{39, 40} type of impregnated porous carbon electrode used in the experiments described in section 2.2a (Electrode No. 16) was prepared in the manner described below.

A 1.0-in. diameter, 0.25-in. thick, disk was machined out of a National Carbon Company, Grade 20, porous graphite block. This material has a porosity of 48%, and an average pore diameter of 140 microns. The disk then underwent treatment as follows:

1. Washed in benzene,
2. Dried in 110°C oven for 1.0 hour,
3. Washed in 30% HNO₃ for 5 minutes,
4. Dried in 110°C oven for 1.0 hour,
5. Impregnated with the catalyst metal's solution (fully immersed to soak),
6. Dried in 110°C oven for 1.0 hour, and
7. Baked in H₂ furnace at 850°C for 1.0 hour, cooled in the same H₂ atmosphere to room temperature.

The composition of the catalyst metal's impregnating solution was

100 cc Distilled Water

5.65g AgNO₃

12.50g Al(NO₃)₃

which yielded a metal loading of the electrode

1.7% by weight Ag

1.76% by weight Al.

The aluminum was then leached out in strong caustic. No attempt was made to find out how the metal was distributed throughout the electrode.

APPENDIX D

CALCULATIONS OF THE TOTAL CURRENT WITHIN A PORE

Choose a pore diameter, say, 30 Å, and material Pt.

Oxygen partial pressure at the pore mouth, 1.0 atm.

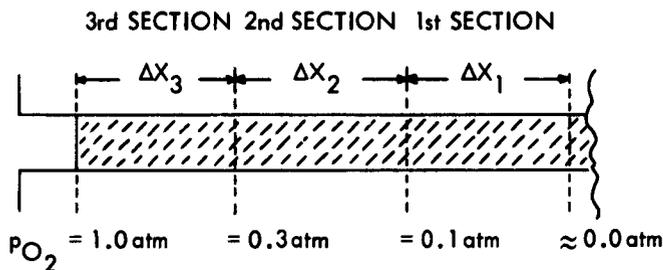
From Fig. 5, on a platinum electrode in 20% KOH, the oxygen electroreduction rates can be read. At an electrode potential of 0.00 volt vs the S. H. E., the corresponding current densities are:

$$3 \times 10^{-4} \text{ amp/cm}^2 \text{ at } 1.0 \text{ atm Oxygen partial pressure}$$

$$1 \times 10^{-4} \text{ amp/cm}^2 \text{ at } 0.2 \text{ atm Oxygen partial pressure}$$

$$5 \times 10^{-5} \text{ amp/cm}^2 \text{ at } 0.1 \text{ atm Oxygen partial pressure}$$

The pore can be divided into sections, for example, in three sections as follows:



First Section

We can approximate the O_2 concentration as being constant throughout, and equivalent to an oxygen partial pressure of $\frac{0.1 + 0}{2} = 0.05$ atm. Then the surface current density, i_s , will be 2×10^{-5} amp/cm². For this section, the length ΔX_1 can be solved for by the approximate relation derived in section 3. 1.

$$\begin{aligned} \Delta X_1 &= \left(\frac{2D_L C_{O_1} F d}{i_{s1}} \right)^{1/2} \\ &= \left(\frac{2(1.8 \times 10^{-5})(2.9 \times 10^{-7})(0.05)(96,500)(3 \times 10^{-7})}{2 \times 10^{-5}} \right)^{1/2} \\ &= 2.74 \times 10^{-5} \text{ cm.} \end{aligned}$$

The total number of moles of O_2 flowing into this section will be

$$N_{\Delta X_1} = \frac{i_{s1} (\Delta X_1) \pi d}{4F} = \frac{(2 \times 10^{-5})(2.74 \times 10^{-5}) \pi 3 \times 10^{-7}}{4(96,500)}$$

$$= 1.34 \times 10^{-21} \text{ g moles/pore-sec.}$$

Second Section

$$pO_2 \text{ average} = \frac{0.3 + 0.1}{2} = 0.2 \text{ atm, } i_{s2} = 1 \times 10^{-4} \text{ amp/cm}^2.$$

Part of the oxygen will travel through the second section to be reduced in the first section, and we desire to determine the oxygen concentration drop, ΔC_{X_1} , that will be needed in the second section to permit this:

$$N_{\Delta X_1} = 1.34 \times 10^{-21} = \frac{D_L (\Delta C_{X_1}) \pi d^2}{\Delta X_2 (4)} = \frac{1.8 \times 10^{-5} (\Delta C_{X_1}) \pi (3 \times 10^{-7})^2}{\Delta X_2 (4)} \quad (D-1)$$

Similarly, as in the first section,

$$\Delta X_2 = \left(\frac{(C_{O_2} - \Delta C_{X_1}) D_L (2) dF}{i_{s2}} \right)^{1/2}$$

$$= \left(\frac{(0.2(2.9 \times 10^{-7}) - \Delta C_{X_1}) 1.8 \times 10^{-5} (2)(3 \times 10^{-7}) 96,500}{1 \times 10^{-4}} \right) \quad (D-2)$$

From Eqs. D-1 and D-2,

$$\Delta X_2 = 3 \times 10^{-5} \text{ cm}$$

$$N_{\Delta X_2} = \frac{(3 \times 10^{-5})(1 \times 10^{-4}) \pi 3 \times 10^{-7}}{(4)(96,500)} = 7.3 \times 10^{-21} \frac{\text{g moles}}{\text{pore-sec}}$$

Third Section

$$pO_2 \text{ average} = \frac{1.0 + 0.3}{2} = 0.65 \text{ atm, } i_{s3} = 2.62 \times 10^{-4} \text{ amp/cm}^2$$

$$N_{\Delta X_{12}} = N_{\Delta X_1} + N_{\Delta X_2} = (1.34 + 7.3) \times 10^{-21} = 8.64 \times 10^{-21} \frac{\text{g moles}}{\text{pore-sec}}$$

$$N_{\Delta X_{12}} = 8.64 \times 10^{-21} = \frac{D_L (\Delta C_{X_{12}}) \pi d^2}{\Delta X_3 (4)} = \frac{\Delta C_{X_{12}}}{\Delta X_3} 1.27 \times 10^{-18} \quad (D-3)$$

Similarly,

$$\Delta X_3 = \left(\frac{(C_{O_3} - \Delta C_{X_{12}})(D_L)(2) dF}{i_{s3}} \right)^{1/2}$$

$$\Delta X_3 = \left(\frac{((0.7) 2.9 \times 10^{-7} - \Delta C_{X_{12}})(1.8 \times 10^{-5})(2) 3 \times 10^{-7}(96,500)}{2.62 \times 10^{-4}} \right)^{1/2} \quad (D-4)$$

From (D-3) and (D-4),

$$\Delta X_3 = 3.86 \times 10^{-5} \text{ cm}$$

$$N_{\Delta X_3} = \frac{(3.86 \times 10^{-4})(2.62 \times 10^{-4}) \pi 3 \times 10^{-7}}{(4)(96,500)}$$

$$= 2.46 \times 10^{-20} \text{ g moles/sec-pore.}$$

The total number of moles of O_2 flowing into the pore will be

$$N_{\Delta X_1} + N_{\Delta X_2} + N_{\Delta X_3} = (2.46 + 0.73 + 0.134) \times 10^{-20}$$

$$= 3.32 \times 10^{-20} \text{ g moles/pore-sec.}$$

The current density per cm^2 of micropore structure will be

$$i_{ps} = \frac{(\Sigma N_{\Delta X_i}) 4F}{(4) d^2} = \frac{3.32 \times 10^{-20} (4)(96,500)}{(4)(3 \times 10^{-7})^2} = 3.56 \times 10^{-2} \text{ A/cm}^2.$$

For other electrode potentials, current-density values can be calculated in a similar fashion.

33. W. McAdams, Heat Transmission (McGraw-Hill Book Company, Inc., New York, 3rd edition, 1954).
34. I. Higuchi, T. Ree, and H. Eyring, J. Am. Chem. Soc. 77, 4969 (1955); 79, 1330 (1957).
35. W. M. Kays and A. L. London, Compact Heat Exchangers (McGraw-Hill Book Company, Inc., New York, 1958).
36. C. N. Satterfield and P. Sarda, Rates of Catalytic Decomposition of Liquid Hydrogen Peroxide on Metal Surfaces, Report No. 58, Office of Naval Research, Contract Nonr 1841(11), Project NR-092-008 (1960).
37. K. Kordesh, Chapter 2, Fuel Cells, edited by C. Young (Reinhold Publishing Corporation, New York, 1960).
38. J. Harned, Am. Chem. Soc. 59, 496 (1937).
39. K. Kordesh, U. S. Patent 2,615,932.
40. K. Kordesh, U. S. Patent 2,669,598.
41. International Critical Tables, Vol. VI (McGraw-Hill Book Company, Inc., New York, 1925).

